Ride Comfort Analysis of Unmanned Mining Vehicles Based on Torque-Compensated Semi-Active Hydro-Pneumatic Suspension

Yu Fu *, Yunfan Li, Qingrong Liu, Yirui Kou

School of Automotive and Traffic Engineering, Jiangsu University, Zhenjiang, China, 212013

* Corresponding Author Email: 18896670776@163.com

Abstract. Under the impetus of the national policy on intelligent mining equipment, the upgrading of the suspension of mining trucks has become a necessary condition to meet the growing demand of open-pit mines. To address the problem of severe vibration and instability caused by complex road surfaces, a semi-active oil-gas suspension control strategy with torque compensation is proposed. A nonlinear dynamic model of the suspension system was established, and its nonlinearity was analyzed using van der Waals equations. To optimize damping parameters in real time, an enhanced skyhook control algorithm with pitch moment and roll moment compensation was proposed. Simulation results show significant improvement under C-class random road excitation: compared with passive suspension, the proposed strategy can reduce vertical acceleration by 18.11%, pitch Angle acceleration by 18.26%, and roll Angle acceleration by 21.22%. On a long slope, the peak pitch and vertical acceleration at the center of gravity were reduced by 22.13% and 19.12%, respectively. This strategy effectively suppresses the larger fluctuations of the vehicle body by optimizing vibration and stability. The study verified the coordinated optimization mechanism between torque compensation and vertical vibration control, providing a theoretical basis for improving the ride and operational safety of mining autonomous trucks under complex conditions.

Keywords: Automatic Mining Trucks, Semi-Active Suspension, Oil-gas Suspension System, Vehicle Posture, Enhanced Skyhook Control Algorithm.

1. Introduction

The autonomous transformation of mining trucks has emerged as a critical technological frontier, driven by national initiatives promoting new energy vehicles and intelligent mining development [1]. Confronting challenges including labor shortages, efficiency limitations of human-operated systems, and inherent safety risks in mining operations, China's strategic goal to achieve intelligent operations in large-scale and high-risk coal mines by 2025 has accelerated policy support and market adoption of autonomous mining trucks (AMTs) [2]. This technological shift demonstrates significant potential to enhance operational efficiency and safety standards.

Accurate trajectory tracking constitutes the fundamental requirement for AMT operations. Previous research has systematically addressed this challenge through multiple approaches: Aydemir et al. [3] established motion planning frameworks for mining truck-trailer systems, while subsequent studies developed nonlinear model predictive control (NMPC) strategies to improve tracking accuracy during high-speed maneuvers and large-steering-angle operations [4]. Liu's research team further enhanced control precision by implementing a particle swarm optimization (PSO)-augmented NMPC strategy for underground vehicles [5]. However, these advancements predominantly concentrate on path tracking performance, with insufficient attention to ride comfort and postural stability under extreme off-road conditions [6].

Mining terrains generate substantial road excitations due to their characteristic ruggedness, severely compromising vehicle stability and ride quality. Gong's research group systematically analyzed posture variations of heavy vehicles across different road classifications and proposed corresponding suspension parameter optimization methods [7].Feng et al. developed electromechanical-coupled dynamic models to quantify road excitation impacts, aligning with

industry electrification trends. Beckers et al [8]. specifically emphasized the critical role of nonlinear dampers in maintaining vehicular stability under severe road impact conditions [9].

Hydro-pneumatic suspensions have become prevalent in heavy-duty mining vehicles owing to their nonlinear stiffness characteristics and adjustable damping capabilities. Substantial research efforts have focused on performance optimization: Wang's fuzzy PID control strategy effectively addresses payload variation challenges [10]. While Sun et al. proposed a grey wolf algorithm-optimized skyhook control method [11]. International researchers have contributed comprehensive analyses through theoretical and experimental investigations of mechanical characteristics [12], ride comfort evaluation metrics [13], and thermal effect mechanisms [14]. These collective efforts have significantly advanced the understanding of hydro-pneumatic suspension dynamics.

Despite technological progress in AMT development, current research priorities remain skewed toward environmental perception, intelligent decision-making, and motion control systems [15]. This emphasis has created notable research gaps regarding ride comfort and postural stability management in unstructured mining terrains. Our study specifically investigates the integrated optimization of ride comfort and posture stability for AMTs equipped with semi-active hydro-pneumatic suspensions under typical mining road excitations. We introduce an innovative moment-compensated skyhook control strategy that enables real-time intelligent regulation of suspension stiffness and damping parameters. The proposed methodology achieves performance enhancement through three key mechanisms: synergistic optimization of vibration suppression and posture stabilization, adaptive response to extreme load variations and terrain conditions, and thermal-stability-aware control implementation.

This research establishes a theoretical foundation for improving all-weather operational efficiency, environmental adaptability, and safety assurance in AMT applications. The findings provide actionable engineering guidelines for developing next-generation intelligent mining equipment.

2. Suspension model and control algorithm model

2.1. Nonlinear damping force of hydro-pneumatic suspension

Damp-adjustable semi-active hydro-pneumatic suspensions can be divided into two types: stepless and continuously adjustable. Among them, the continuously adjustable type has a fast response and high control accuracy, and is suitable for high-performance vehicles or complex road conditions. The damping coefficient is mainly adjusted in real time through electronic control valves, magnetorheological, and electrostatic liquids. There are two main types of shock absorbers based on the principle of controllable viscosity: current variable (ER) and magnetorheological (MR).

2.1.1. Semi-active oil-gas suspension structure

The system features an integrated gas-hydraulic coupling design, with core components including the actuator assembly, pressure cylinder block, high-pressure air chamber, top cover assembly, double-acting piston module, external circulation pipeline, and electronically controlled proportional throttle valve. The structure is simplified as shown in Figure 1 below.**Figure 1.** Basic structure of semi-automatic hydro-pneumatic suspension1

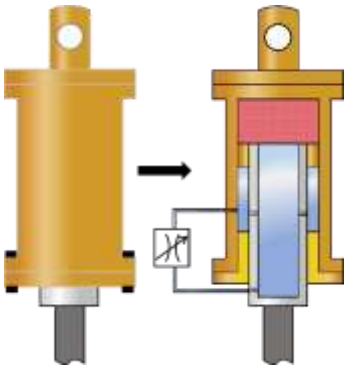

Figure 1. Basic structure of semi-automatic hydro-pneumatic suspension1

According to the movement characteristics of the hydro-pneumatic suspension, its working process can be divided into two stages: compression and extension. During compression, the actuator assembly slides upward along the inner wall of the cylinder, resulting in a reduction in the effective volume of the high-pressure chamber and an increase in air pressure. The variable cross-section throttle valve is controlled by an electromagnetic actuator with a stepless regulation function, which can precisely control the dynamic damping force. When the rod is stretched, the reverse displacement of the actuator assembly causes the volume expansion pressure of the air chamber to decrease and the oil pressure in the annular cavity to increase.

2.1.2. Analysis of nonlinear characteristics of semi-active hydro-pneumatic suspension

Compared with the traditional passive suspension, the semi-active hydro-pneumatic suspension achieves the adjustment of the damping force by improving the shock absorber structure. After installing the electromagnetic proportional valve, the flow cross-sectional area of the actuator is adjusted in real time, and the system can dynamically select the damping parameters.

The nonlinear dynamic characteristics of the semi-active oil-gas suspension are mainly reflected in two parts: the nonlinear damping force and the nonlinear gas elastic force

Therefore, the kinetic model should be based on the van der Waals equation kinetic model. To simplify the modeling complexity, the following model assumptions are made:

(1) The oil and gas suspension is well sealed, and leakage at the interface is negligible.

(2) Assume that temperature changes in the medium have no significant effect on the physical parameters.

(3) The temperature remains constant during repeated nitrogen compression processes.

(4) Take the effective radius of the nitrogen molecule as 0.365 nm.

(5) Ignore the effect of inertial mass on dynamic response and focus only on oil pressure analysis.

(6) The volumetric modulus of the hydraulic oil is close to that of the ideal fluid, and the oil is considered incompressible.

(7) The proportional solenoid valve has no leakage, and the flow resistance can be ignored.

(8) Frictional losses of the moving pairs are not considered in the model.

(9) Gas-liquid dissolution processes are not taken into account.

(10) The elastic deformation of the structure is within an acceptable margin of error.

(11) Ignore the pressure drop error in the pipe.

2.1.3. Shock absorbers compress the damping force

Figure 2. Compression stroke2

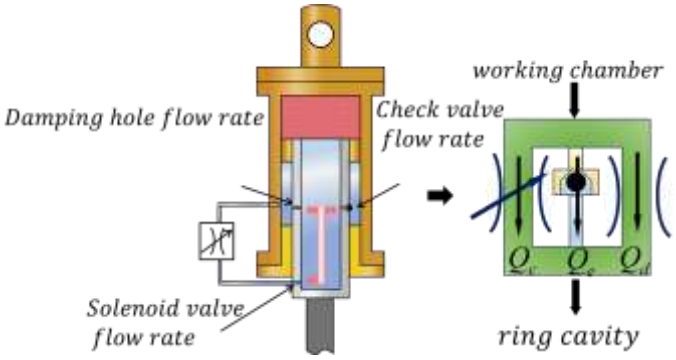

Figure 2. Compression stroke2

The formula for damping hole flow is as follows:

$$Q_d = K_d S_d \left(\frac{2\Delta P_d}{\rho} \right)^{\frac{1}{n_d}} \tag{1}$$

Where Q_d is the flow rate through the damping orifice, K_d is the flow coefficient of the damping orifice, S_d is the cross-sectional area of the damping oorificessure difference across the damping orifice, ρ is the fluid density, and n_d is an empirical value. Since the damping orifice in the hydro-pneumatic suspension is a long, slender hole, K_d is taken as 0.75, and n_d is taken as 2.

Check valve flow depends on the overflow area of the check valve. As shown in Figure 3, the overflow area is equivalent to a torus on a cone, and when expanded, a circular sector area can be calculated to obtain the overflow area.**Figure 3.** Schematic diagram of the overflow area of the check valve3

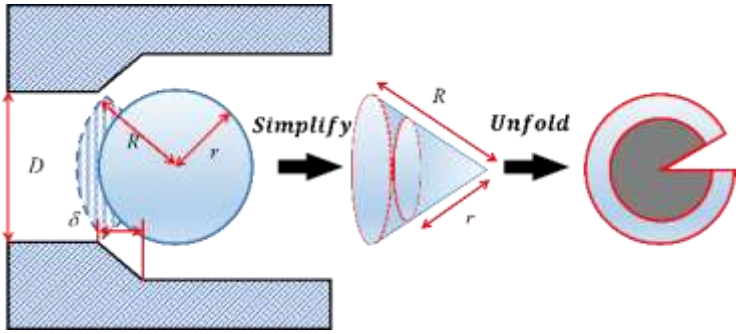

Figure 3. Schematic diagram of the overflow area of the check valve3

As is shown in Figure 3, δ is the lift of the check valve when it is open, r is the diameter of the sealing steel ball, and the port diameter of the check valve is D. The minimum distance R from the edge of the check valve port to the center of the sealing steel ball can be calculated. The developed annular area corresponds to the central angle θ of the check valve's flow area, from which the flow area S_c can be determined.

$$\begin{cases} R = \sqrt{r^2 + 2\delta\sqrt{r^2 - D^2/4} + \delta^2} \\ \theta = \pi D / R \\ S_c = \dfrac{1}{2}\theta\left(R^2 - r^2\right) \end{cases} \tag{2}$$

Organize to obtain the check valve flow formula:

$$S_c = \frac{\dfrac{\pi}{2} D\left(2\delta\sqrt{\left(4r^2 - D^2\right)/4} + \delta^2\right)}{\sqrt{r^2 + 2\delta\sqrt{\left(4r^2 - d^2\right)/4} + \delta^2}} \tag{3}$$

$$\mathrm{Q}_c = K_c S_c \left(\frac{2\Delta P_c}{\rho}\right)^{\frac{1}{n_c}} \tag{4}$$

Where Q_s is the flow rate through the check valve, K_s is the flow coefficient of the check valve, S_s is the flow area of the check valve, P_2 is the pressure difference across the check valve, and n_s is an empirical value, taken as 2.

The formula for calculating the flow rate at the throttle orifice of the solenoid valve is as follows:

$$Q_e = K_e S_e \left(\frac{2\Delta P_e}{\rho}\right)^{\frac{1}{n_e}} = \frac{K_e \pi D_e{}^2 x_e}{4}\left(\frac{2\Delta P_e}{\rho}\right)^{\frac{1}{n_e}} \tag{5}$$

Where Q_e is the flow rate through the throttle orifice of the electro - magnetic proportional valve, K_e is the flow coefficient of the throttle orifice of the electro - magnetic valve, taken as 1.75 for a long - slender orifice; S_e is the area of the throttle orifice of the electro - magnetic valve; D_e is the diameter of the throttle orifice of the electro - magnetic valve; x_e is the relative opening of the

throttle orifice of the electro - magnetic valve; P_e is the pressure difference across the throttle orifice of the electro - magnetic valve; and n_e is an empirical value, usually taken as 2.

The three ports are connected in parallel, and the relationship between flow and pressure difference can be further derived by the continuity equation.

$$\begin{cases} \Delta P_c = \Delta P_d = \Delta P_e \\ Q = Q_c + Q_d + Q_e \\ Q = A_2 \dot{x} \end{cases} \tag{6}$$

The damping force expression for the compressed stroke is as follows:

$$F_c = \frac{\rho A_2^3 \dot{x}^2}{2\left[n\left(K_c S_c + K_d S_c\right) + K_e \pi D_e^2 x_e / 4\right]^2} \tag{7}$$

2.1.4. Shock absorber stretch damping force

When constructing the dynamic model of the extension process, the modeling idea of the compression stroke can be borrowed. The conduction characteristics of the hydraulic oil line under this condition can be seen in Figure 4.

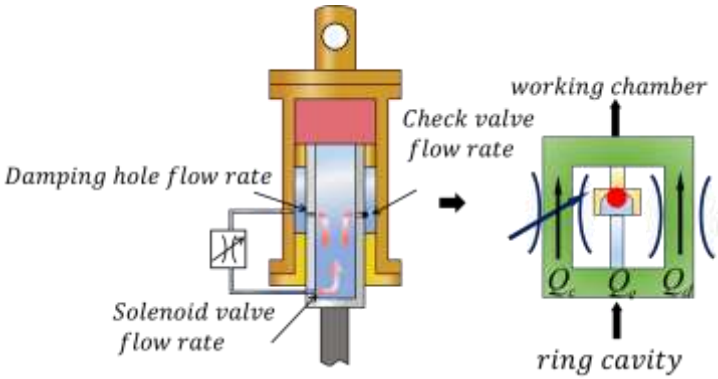

Figure 4. Stretch stroke4

During the stretch, only the solenoid flow valve and the damping hole are open. The mathematical relationship between flow and pressure is:

$$\begin{cases} \Delta P = \Delta P_e = \Delta P_d \\ Q = Q_e + Q_d = A_2 \dot{x} \end{cases} \tag{8}$$

The tension stroke damping force is shown as follows:

$$F_s = \frac{\rho A_2^3 \dot{x}^2}{2\left(nK_d S_d + + K_e \pi D_e^2 x_e / 4\right)^2} \tag{9}$$

2.1.5. Elastic force modeling

The elastic force of the semi-active oil-gas suspension is mainly generated by high-pressure nitrogen, showing obvious nonlinearity. The effective radius of nitrogen molecules at high pressure must be taken into account, and the following mathematical model was established using van der Waals equations:

$$\left(P + \frac{m^2}{M^2}\frac{a}{V^2}\right)\left(V - \frac{m}{M}b\right) = \frac{m}{M}R'T \tag{10}$$

Where P is the pressure at a given moment, V is the gas volume at a given moment, M is the molar mass of nitrogen molecules, a is a constant reflecting the influence of intermolecular forces

on pressure, b is the effective volume per mole of gas, and R' is the universal gas constant, taken as $8.31J/(mol \cdot K)$. Under the working pressure of the hydro-pneumatic suspension, a is typically taken as $0.84 \cdot 10^5 Pa \cdot L^2/mol^2$, and b is typically taken as $0.0305\ L/mol$.

2.2. Road excitation model

2.2.1. Straight pavement model

The pavement grades are divided into a total of eight grades, with the pavement unevenness gradually increasing. In this paper, grade C pavement is used as the pavement excitation source. $A-H$ After smoothing the power spectral density, Equation (1) is the fitting expression. After the inverse Fourier transform, Equation (2) is obtained, which is the expression of the pavement excitation in the time domain.

$$G_q(n) = G_q(n_0)(\frac{n}{n_0})^{-W} \tag{11}$$

$$Z_r(t) = 2\pi n_0 \sqrt{G_q(n_0)u} \int_0^t \omega(t)dt \tag{12}$$

The two-sided correlation of pavement excitation mainly stems from the unity of road construction characteristics and load action mechanism.

$$\begin{cases} \gamma^2(n) = \dfrac{\left|S_{q_{left}q_{rigth}}(n)\right|^2}{S_{q_{left}}(n)S_{q_{rigth}}(n)} \\ \gamma(n) = e^{-kdn} \end{cases} \tag{13}$$

Where $S_{qlfet}(n)$ is the power spectral density of the left wheel excitation, $S_{qright}(n)$is the power spectral density of the right wheel excitation, $S_{qlfetqrigt}(n)$ is the cross-power spectral density between the left and right wheel excitations, n is the circular frequency, ρ is the fitting parameter, typically taken as 0.5 for mining trucks with a larger wheelbase, d is the distance between the left and right wheels, and v is the vehicle speed.

2.2.2. Long slope road surface model

The model simulates the dynamic response of a vehicle to a long slope bump while driving, and the mathematical expression of the road surface is as follows:

$$H = 60\left(1-\cos\left(2\pi\frac{x}{4000}\right)\right) \tag{14}$$

2.3. Ceiling control algorithm based on attitude compensation

2.3.1. Dynamic model of the vehicle's seven-degree-of-freedom suspension

Compared with the single-wheel two-degree-of-freedom and two-wheel models, the seven-degree-of-freedom whole vehicle model gives a clearer picture of how the suspension affects the flatness of the vehicle body. The seven-degree-of-freedom dynamics model based on semi-active hydro-pneumatic suspension relies on the following assumptions:

(1) Treat the fuselage as a rigid body, ignoring the twisting and bending of the fuselage;

(2) The vehicle only considers horizontal movement (lateral, longitudinal, yaw), ignoring vertical runout;

(3) The stiffness and damping of the suspension are within the linear range;

(4) Considering only the vertical tire force, it is considered a coil spring;

(5) Do not consider the tire's swing

Retaining the main dynamic elements results in a simplified diagram of the seven-degree-of-freedom suspension model, as shown in Figure 5:**Figure 5.** Simplified model of the whole vehicle

The seven-degree-of-freedom model of the vehicle is as follows:5

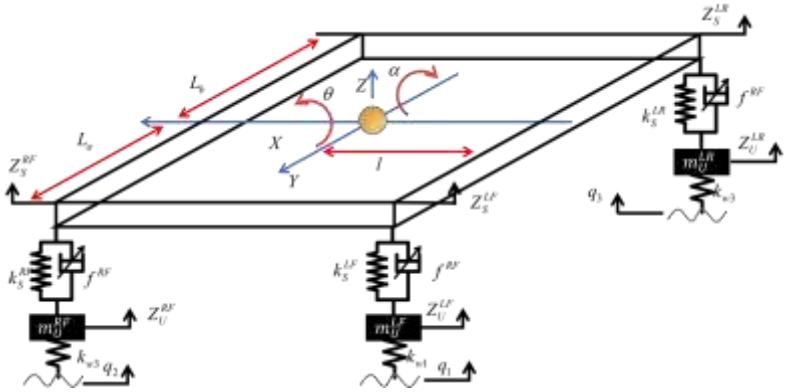

Figure 5. Simplified model of the whole vehicle

The seven-degree-of-freedom model of the vehicle is as follows:5

$$\begin{cases} I_{XX}\ddot{\theta} = \left[\left(Z_U^{LR} - Z_U^{LR}\right)k_S^{LR} + f^{LR} + \left(Z_U^{RR} - Z_U^{RR}\right)k_S^{RR} + f^{RR}\right]L_b - \left[\left(Z_S^{RF} - Z_U^{RF}\right)k_S^{RF} + f^{RF} + \left(Z_U^{LF} - Z_U^{LF}\right)k_S^{LF} + f^{LF}\right]L_a \\ I_{YY}\ddot{\alpha} = \left[\left(Z_S^{RF} - Z_U^{RF}\right)k_S^{RF} + f^{RF} + \left(Z_U^{RR} - Z_U^{RR}\right)k_S^{RR} + f^{RR}\right]l - \left[\left(Z_U^{LR} - Z_U^{LR}\right)k_S^{LR} + f^{LR} + \left(Z_U^{LF} - Z_U^{LF}\right)k_S^{LF} + f^{LF}\right]l \\ m\ddot{Z} = \left(Z_U^{LR} - Z_U^{LR}\right)k_S^{LR} + f^{LR} + \left(Z_U^{RR} - Z_U^{RR}\right)k_S^{RR} + f^{RR} + \left(Z_S^{RF} - Z_U^{RF}\right)k_S^{RF} + f^{RF} + \left(Z_U^{LF} - Z_U^{LF}\right)k_S^{LF} + f^{LF} \end{cases} \quad (15)$$

Here, Z_S^{ij} represents the vertical displacement of the suspension mass at the four wheels; Z_U^{ij} represents the vertical displacement of the unsprung mass at the four wheels; Z is the vertical displacement of the center of mass; q is the vertical road excitation at the four wheels; K_S^{ij} is the stiffness of the suspension springs; K_T^{ij} is the stiffness of the wheel springs; θ is the pitch angle of the vehicle body; α is the roll angle of the vehicle body; l is the track width; L_a and L_b are the distances from the center of mass to the front and rear axles, respectively. f^{ij} is the active force of the suspension. The motion of the vehicle body can be simplified to the vertical movement of the center of mass and the rotation around the longitudinal (Y-axis) and transverse (X-axis) axes. The equation of motion for the center of mass is as follows:

$$\begin{cases} Z_S^{LF} = -\theta \square L_a - \alpha \square l \\ Z_S^{RF} = -\theta \square L_a + \alpha \square l \\ Z_S^{LR} = +\theta \square L_b - \alpha \square l \\ Z_S^{RR} = +\theta \square L_b + \alpha \square l \end{cases} \quad (16)$$

The equation of motion for non-suspended masses can be expressed as:

$$\begin{cases} \ddot{Z}_U^{LF} = k_{w1}\left(q_1 - Z_U^{LF}\right) - k_S^{LF}\left(Z_U^{LF} - Z_S^{LF}\right) - f^{LF} \\ \ddot{Z}_U^{RF} = k_{w2}\left(q_2 - Z_U^{RF}\right) - k_S^{RF}\left(Z_U^{RF} - Z_S^{RF}\right) - f^{RF} \\ \ddot{Z}_U^{LR} = k_{w3}\left(q_3 - Z_U^{LR}\right) - k_S^{LR}\left(Z_U^{LR} - Z_S^{LR}\right) - f^{LR} \\ \ddot{Z}_U^{RR} = k_{w4}\left(q_4 - Z_U^{RR}\right) - k_S^{RR}\left(Z_U^{RR} - Z_S^{RR}\right) - f^{RR} \end{cases} \quad (17)$$

2.3.2. Torque compensation control algorithm design based on the ceiling algorithm

Using the Skyhook control strategy, the damping force expression is as follows:

$$\begin{cases} f^{LF} = -C_{Sky}^{F} \cdot \dot{Z}_S^{LF} \\ f^{RF} = -C_{Sky}^{F} \cdot \dot{Z}_S^{RF} \\ f^{LR} = -C_{Sky}^{R} \cdot \dot{Z}_S^{LR} \\ f^{RR} = -C_{Sky}^{R} \cdot \dot{Z}_S^{RR} \end{cases} \tag{18}$$

Body attitude control not only needs to control the single-wheel semi-active hydro-pneumatic suspension, but also needs to consider the roll and pitch moments that the body is subjected to, thereby reducing the pitch and roll movements of the body, as shown in Figure 6.

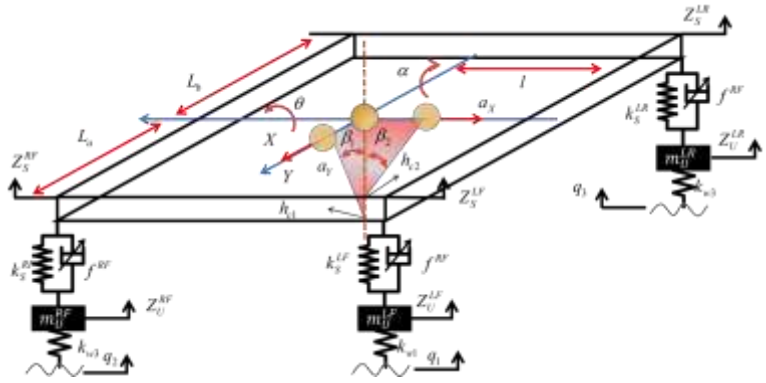

Figure 6. Diagram of torque compensation6

In Figure 6, the height of the body pitch and roll center, for body pitch and roll angles, for longitudinal and lateral acceleration of the vehicle body.

In the Figure, h_{c1} and h_{c2} represent the heights of the pitch and roll centers of the vehicle body; β_1 and β_2 represent the pitch and roll angles of the vehicle body; a_X and a_Y represent the longitudinal and lateral accelerations of the vehicle body.

The roll and pitch of the vehicle body are the result of the combined action of three moments: the inertial moment M_a caused by acceleration, the moment M_d caused by the transverse and longitudinal displacement of the center of mass, and the load transfer moment $M_s$caused by the deformation of the suspension.

Expressions for the three torques are as follows:

$$\begin{cases} M_{aX} = m \cdot a_X \cdot h_g \\ M_{aY} = m \cdot a_Y \cdot h_g \end{cases} \tag{19}$$

$$\begin{cases} M_{dX} = m \cdot g \cdot (h_g - h_{c1}) \cdot \beta_1 \\ M_{dY} = m \cdot g \cdot (h_g - h_{c2}) \cdot \beta_2 \end{cases} \tag{20}$$

$$\begin{cases} M_{sX} = (F_{LF} + F_{RF}) \cdot L_a - (F_{LR} + F_{RR}) \cdot L_b \\ M_{sY} = (F_{LF} + F_{LR} - F_{RF} - F_{RR}) \cdot l \end{cases} \tag{21}$$

In order to balance the above three moments, compensatory force Δf and compensatory moment M_c should be used according to the roll and pitch moments. The expressions are as follows:

$$\begin{cases} M_{cX} = (\Delta f_{LF} + \Delta f_{RF}) \cdot L_a - (\Delta f_{LR} + \Delta f_{RR}) \cdot L_b \\ M_{aX} + M_{dX} - M_{sX} - M_{cX} = 0 \\ M_{cY} = (\Delta f_{LF} + \Delta f_{LR}) \cdot l - (\Delta f_{RF} + \Delta f_{RR}) \cdot l \\ M_{aY} + M_{dY} - M_{sY} - M_{cY} = 0 \end{cases} \tag{22}$$

3. Simulation results

The road excitation of the four wheels is obtained through MATLAB/Simulink, as shown in Figures 7 to 8.

Figure 7. Road excitation of the left front wheel and the right front wheel

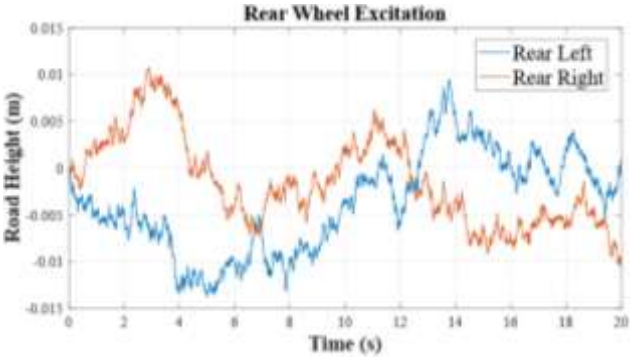

Figure 8. Left rear wheel and left rear wheel road excitation

The excitations of the front and rear axles are delayed in the time domain, while the left and right excitations show spatial coherence. To verify whether the semi-active hydro-pneumatic suspension with torque compensation control can effectively suppress body pitch and roll, Matlab/Simulink simulation was carried out on a Class C road with a speed of 50 km/h. Observations of vertical acceleration and pitch/roll motion were analyzed (Figure 9-11). Compared with the traditional hook damping algorithm, the torque compensation algorithm achieved significant improvements: the vertical acceleration of the vehicle body decreased by 18.11%, the pitch Angle acceleration decreased by 22.13%, and the roll Angle acceleration decreased by 21.22%. The time-domain and frequency-domain curves show that the compensated torque does not diminish the effectiveness of vertical control in enhancing ride comfort; Instead, it is compatible.

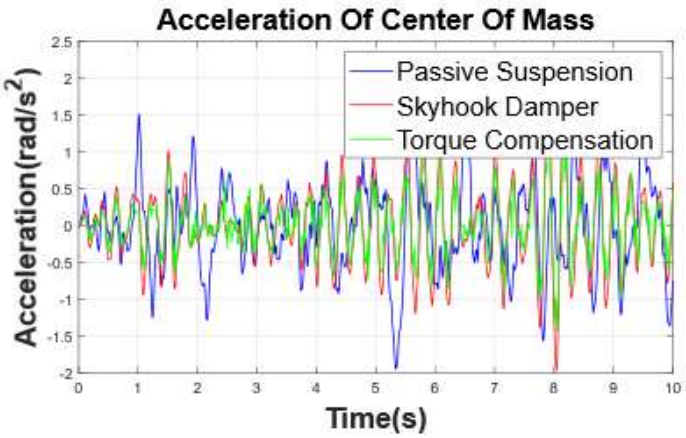

Figure 9. Comparison of the vehicle's center of mass acceleration

7

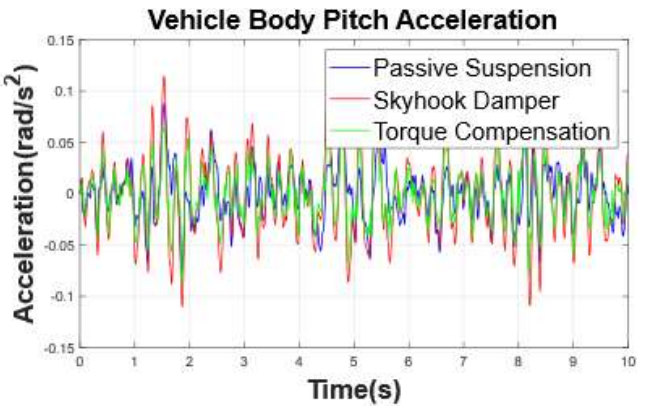

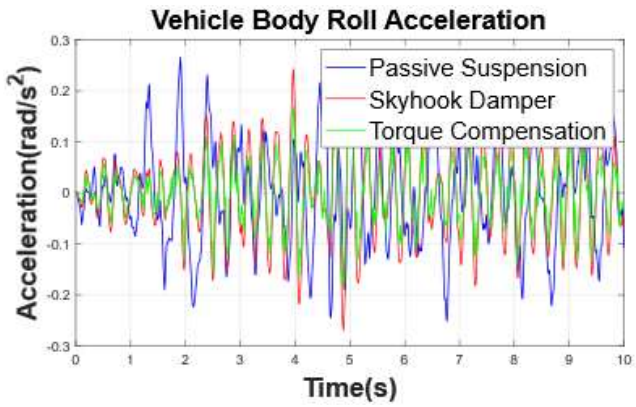

Figure 10. Comparison of body pitch acceleration

Figure 11. Comparison of body roll acceleration

Under the influence of a long slope, the vertical acceleration and pitch motion of the vehicle body are observed.

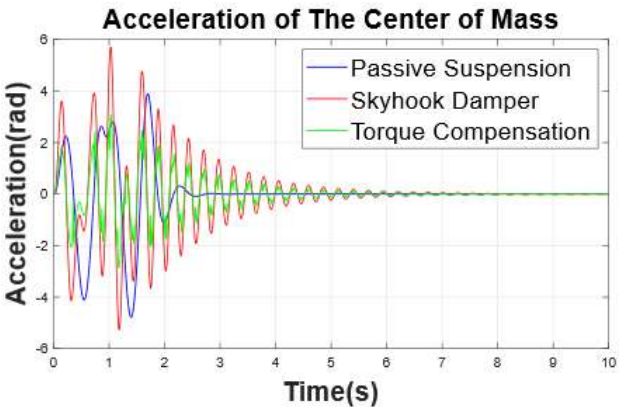

Figure 12. Comparison of the car's pitch acceleration

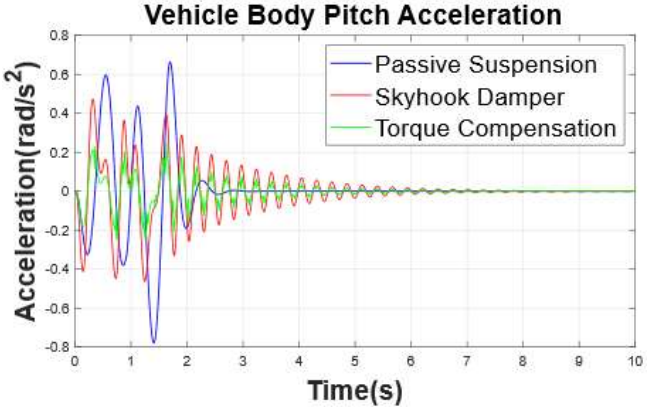

Figure 13. Comparison of the centroid acceleration of the vehicle body

As shown in Figures 12 to 13, compared with the traditional passive suspension system, the attitude compensation semi-active suspension system significantly reduces the root mean square (RMS) values of pitch Angle acceleration and centroid vertical acceleration. Notably, its control performance improved by 19.6 percent and 22.3 percent, respectively, compared to the baseline semi-active suspension. The simulation results show that the suspension system with an integrated torque compensation mechanism effectively suppresses body pitch when crossing long slopes, significantly improving ride comfort and attitude control efficiency.

4. Conclusion

In this study, we've explored the ride comfort and pose stability of AMTs with semi-active hydro-pneumatic suspensions under typical mining road excitation. An innovative torque-compensated hook control strategy is proposed, enabling real-time intelligent adjustment of suspension stiffness and damping parameters.

Simulation results indicate that, compared to passive suspension, our strategy significantly reduces vertical, pitch Angle, and roll Angle acceleration under C-class random road excitation. It also effectively lowers the peak pitch and vertical acceleration at the center of gravity on long slopes. This shows it can suppress vehicle body fluctuations and enhance ride comfort and stability.

But there's room for improvement. The model could be refined by incorporating more real-world factors like tire flexibility and suspension geometry changes. The control strategy's performance in extreme scenarios such as sudden large bumps also needs further testing and optimization.

Future research can focus on developing more advanced control algorithms with machine learning techniques to enhance adaptability. Experimental validation on actual mining trucks is also needed to verify the practical effectiveness and robustness of the proposed strategy.

References

[1] Zang Jinhuan, Li Chunling. Interpretation of the Adjustment of the "Development Plan for the New Energy Vehicle Industry (2021-2035)" [J]. Automotive technicians, 2021, (Z1): 32 - 34.

[2] Guiding Opinions on Accelerating the Intelligent Development of Coal Mines by the National Development and Reform Commission, the National Energy Administration, the Ministry of Emergency Management, the National Coal Mine Safety Supervision Bureau, the Ministry of Industry and Information Technology, the Ministry of Finance, the Ministry of Science and Technology, and the Ministry of Education [J] China Work Safety, 2020, 15 (03): 5.

[3] Aydemir E, Unel M. Motion Planning and Path Following for Autonomous Navigation and Reversing of a Full-Scale Mining Truck and Trailer System [J]. International Journal of Automotive Technology, 2024: 1 - 12.

[4] Li Z, Wang P, Cai S, et al. NMPC-based controller for vehicle longitudinal and lateral stability enhancement under extreme driving conditions[J]. ISA transactions, 2023, 135: 509 - 523.

[5] Liu Y, Peng P, Wang L, et al. PSO-NMPC control strategy-based path tracking control of mining LHD (scraper) [J]. Scientific Reports, 2024, 14 (1): 28516.

[6] Tian B, Yang J, Zhang C, et al. Autonomous Driving in Underground Mines Via Parallel Driving Operation Systems: Challenges, Frameworks and Cases Study[J]. IEEE Transactions on Intelligent Vehicles, 2024.

[7] Chen H, Gong M, Zhao D, et al. Body attitude control strategy based on road level for heavy rescue vehicles [J]. Part D: Journal of Automobile Engineering, 2021, 235 (5): 1351 - 1363.

[8] Feng Guizhen, Li Shaohua, Zhao Wenzhong. Mechatronic Coupling Modeling and Nonlinear Vibration Analysis of Electric Vehicle-Road System [J]. Vibration and Shock, 2021, 40 (14): 18 - 26, 76.

[9] Beckers C J J, Besselink I J M, Nijmeijer H. Quantification of energy losses in suspension dampers and its effects on rolling resistance[J]. Vehicle System Dynamics, 2025: 1 - 21.

[10] Wang Ying. Analysis and Optimization of Hydro-Pneumatic Spring for Mining Vehicle Ride Comfort [D]. Baotou: Inner Mongolia University of Science and Technology, 2019.

[11] Sun Dong, Wang Ruochen, Ding Renkai, et al. Semi-Active Control of Hydro-Pneumatic Suspension for Mining Dump Trucks Based on Grey Wolf Algorithm [J]. China Mechanical Engineering, 2023, 34 (4): 490 - 497.

[12] Sun Dong, Wang Ruochen, Ding Renkai, et al. Semi-active Control of hydro-Pneumatic Suspension for Mining Dump Trucks Based on Grey Wolf Algorithm [J]. China Mechanical Engineering, 2023, 34 (04): 490 - 497.

[13] Yang J, Yin Y, Rakheja S, et al. Mechanics Characteristics of a Kind of Hydro-pneumatic Suspension[J]. Nonlinear Dynamics, 2019, 95 (2): 407 - 419.

[14] Ha D V, Van Cuong B, Hien V T. Performance evaluation of a novel hydro-pneumatic suspension system of a heavy truck on ride comfort [C]//E3S Web of Conferences. EDP Sciences, 2021, 304: 01009.

[15] Sun A, Zhao Z, Li Y, et al. Temperature rise and suspension dynamic characteristics of semi-active hydro-pneumatic suspension based on thermodynamics and heat transfer [J]. Proceedings of the Institution of Mechanical Engineers, Part C: Journal of Mechanical Engineering Science, 2024: 09544062241238862.

[16] Tian Chen, Ding Zhen, Li Zhenjiang, et al. Overall Design of Unmanned Transportation System in Mining Area [J]. Industrial and Mining Automation, 2022, 48 (09): 109 - 115.